

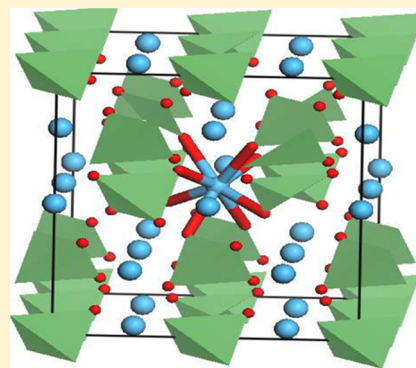
# High-Pressure Structural Stability and Optical Properties of Scheelite-type $\text{ZrGeO}_4$ and $\text{HfGeO}_4$ X-ray Phosphor Hosts

G. Shwetha,<sup>†</sup> V. Kanchana,<sup>\*†</sup> K. Ramesh Babu,<sup>‡</sup> G. Vaitheeswaran,<sup>‡</sup> and M. C. Valsakumar<sup>§</sup>

<sup>†</sup>Department of Physics, Indian Institute of Technology Hyderabad, Ordnance Factory Estate, Yeddumailaram-502 205, Andhra Pradesh, India

<sup>‡</sup>Advanced Centre of Research in High Energy Materials (ACRHEM), and <sup>§</sup>School of Engineering Sciences and Technology (SEST), University of Hyderabad, Prof. C. R. Rao Road, Gachibowli, Hyderabad-500 046, Andhra Pradesh, India

**ABSTRACT:** Ab initio calculations were performed on the scheelite-type  $\text{MGeO}_4$  ( $\text{M} = \text{Hf}$  and  $\text{Zr}$ ) compounds, which find a wide range of applications such as in X-ray imaging. We have studied the high-pressure structural stability, elastic constants, electronic structure, and optical properties of these compounds through density functional theory calculations. Two different density functional approaches, plane wave pseudopotential method (PW-PP) and full potential linearized augmented plane wave method (FP-LAPW), were used for the present study. The ground-state structural and vibrational properties are calculated and found to be in good agreement with experimental data. The compressibility of Zr and Hf germanates is found to be anisotropic as the  $a$ -axis is less compressible over the  $c$ -axis due to the presence of Ge–O bonds along the  $a$ -axis, which is further confirmed from the ordering of the elastic constants that follows  $C_{11} > C_{33}$ . The electronic structure of the compounds has been calculated through recently developed Tran Blaha-modified Becke Johnson potential. The calculated electronic structure shows that the compounds are insulators with a gap of 5.39 eV for  $\text{ZrGeO}_4$  and 6.25 eV for  $\text{HfGeO}_4$ , respectively. Optical anisotropy of these compounds is revealed from the computed optical properties such as complex dielectric function, refractive index, and absorption coefficient. In addition, it is observed that Ti-doped  $\text{ZrGeO}_4$  and  $\text{HfGeO}_4$  turn out to be good phosphors as the pristine compounds have an energy gap greater than the visible range; upon Ti doping, the band gap reduces, and, as a result, emission spectra occur in the visible region and are well explained in the present study.



## INTRODUCTION

Phosphors have a wide range of applications in X-ray imaging, detection, fluoroscopy, etc. Phosphors are used in the medical field particularly in X-ray imaging. The role of these phosphors is to reduce the exposure to X-rays while ensuring the sharpness of the image. To increase the sharpness of the image, we need higher density phosphor with sufficient conversion efficiency. A good X-ray phosphor must be a good absorber of X-ray, with high density and high luminescence efficiency.<sup>1–3</sup> Over the past few decades, several X-ray phosphors such as  $\text{BaFCl}$ ,  $\text{Gd}_2\text{O}_2\text{S}$ ,  $\text{Ln}_2\text{O}_3$ ,  $\text{Sr}_2\text{CeO}_4$ ,  $\text{AB}_2\text{O}_4$  ( $\text{A} = \text{Sr}$ ,  $\text{Zn}$ , and  $\text{Ca}$ ;  $\text{B} = \text{Ga}$ ,  $\text{In}$ ,  $\text{Y}$ , and  $\text{Al}$ ),  $\text{LuTaO}_4\text{:Nb}$ ,  $\text{Hf}_3\text{SnO}_8\text{:Nb}$ ,  $\text{BaHfO}_3$ , and  $\text{HfO}_2\text{:Ti}$  were developed.<sup>1,2</sup> It is well-known that scheelite-type  $\text{ABO}_4$  compounds can serve as good X-ray phosphors. Among the  $\text{ABO}_4$  compounds, germanates of Zr and Hf possess high density and high conversion efficiency, which enables them to be used as X-ray phosphors. When doped with an impurity atom such as Ti, both  $\text{ZrGeO}_4$  and  $\text{HfGeO}_4$  are found to act as high density X-ray phosphors.<sup>2,4</sup> These germanates have also been used as solid-state scintillators,<sup>5</sup> heterogeneous catalysts,<sup>6</sup> and laser-host materials.<sup>7</sup>

The scientific research on the scheelite-type compounds is mainly focused on the structural stability of the compounds under high pressure.<sup>8–12</sup> These studies concluded that the

scheelite-structured compounds transform to monoclinic structure under high pressure. In contrast to these oxides, germanates of Zirconium and Hafnium have been relatively less studied both from theory and from experiment. Panchal et al. experimentally reported the equation of state (EOS) of  $\text{ZrGeO}_4$  and  $\text{HfGeO}_4$  up to the pressure of 20 GPa.<sup>13</sup> The study reveals that both of the compounds do not undergo any phase transition up to the pressure of 20 GPa, in contrast to that of  $\text{ThGeO}_4$ ,<sup>14</sup> which undergoes phase transition from scheelite structure to monoclinic fergusonite structure. This strongly suggests that there is a clear need to understand the high-pressure structural stability of germanates of zirconium and hafnium from a theoretical point of view to address the peculiar high-pressure characteristics.

Theoretical study based on density functional theory calculations is an effective way to understand the properties of solid materials at ambient as well as high pressures. In this present work, we aim to understand the high-pressure structural stability of  $\text{ZrGeO}_4$  and  $\text{HfGeO}_4$  and also shed light on the optical properties with the help of electronic structure by

Received: December 7, 2013

Revised: January 13, 2014

Published: January 28, 2014



performing the first principles density functional calculations. In addition, the main goal of the present work lies in highlighting the effect of Ti doping in  $\text{ZrGeO}_4$  and  $\text{HfGeO}_4$  as they are claimed to be good phosphors. The rest of this Article is organized as follows: Section 2 deals with the computational details, results and discussion are given in section 3, and we end this Article with the conclusions in section 4.

## COMPUTATIONAL DETAILS

The crystal structure, elastic, and vibrational properties were calculated using the Cambridge Sequential Total Energy package.<sup>15–17</sup> We have used Vanderbilt-type ultrasoft pseudopotentials<sup>18</sup> with a planewave expansion of the wave functions. The electronic wave functions were obtained using the density mixing scheme,<sup>19</sup> and the structures were relaxed using the Broyden, Fletcher, Goldfarb, and Shannon (BFGS) method.<sup>20</sup> The exchange–correlation potential of Ceperley and Alder<sup>21</sup> parametrized by Perdew and Zunger<sup>22</sup> in the local density approximation (LDA) and also the generalized gradient approximation (GGA) with the Perdew–Burke–Ernzerhof (PBE) parametrization<sup>23</sup> was used to describe the exchange–correlation potential. The pseudo atomic calculations were performed for Zr  $4d^25s^2$ , Hf  $5d^26s^2$ , Ge  $4s^24p^2$ , and O  $2s^22p^4$ . The Monkhorst–Pack scheme of  $k$ -point sampling was used for integration over the Brillouin zone.<sup>24</sup> The convergence criteria for structure optimization and energy calculation were set to ultra fine quality. We have a cutoff energy of 420 eV and  $4 \times 4 \times 4$   $k$ -points grid for all of the calculations. In the geometry relaxation, the self-consistent convergence threshold on the total energy is  $5 \times 10^{-7}$  eV/atom, and the maximum force on the atom is  $10^{-4}$  eV/Å. The elastic constants are calculated for the optimized crystal structure at ambient conditions by using the volume-conserving strain technique<sup>25</sup> as implemented in CASTEP code. We have relaxed the internal coordinates of the strained unit cell to arrive at the elastic constants.

The electronic structure and optical properties have been calculated by using the full-potential linearized augmented planewave method as implemented in WIEN2k code<sup>26,27</sup> by using the origin choice of 2. For the calculation of electronic structure, we have used a  $10 \times 10 \times 10$   $k$ -grid with 144  $k$ -points in the irreducible Brillouin zone (IBZ) and  $18 \times 18 \times 18$   $k$ -grid with 780  $k$ -points in IBZ for the calculation of optical properties for the  $k$ -space integration. We have used the convergence parameter  $R_{\text{MT}}K_{\text{max}} = 9$ , where  $K_{\text{max}}$  is the planewave cutoff and  $R_{\text{MT}}$  is the smallest of all atomic sphere radii, and the muffin-tin radius was assumed to be 2.13, 1.80, and 1.54 au for Zr, Ge, and O elements, respectively, in the case of  $\text{ZrGeO}_4$  compound, and 2.12, 1.87, and 1.47 au for Hf, Ge, and O, respectively, for the compound  $\text{HfGeO}_4$ . Electronic structure calculations were performed using the Perdew–Burke–Ernzerhof (PBE),<sup>23</sup> Engel–Vosko,<sup>28</sup> and Tran and Blaha modified Becke–Johnson potential (TB-mBJ).<sup>29,30</sup> To study the effect of Ti doping in  $\text{ZrGeO}_4$  and  $\text{HfGeO}_4$ , a supercell of size  $2 \times 1 \times 1$  has been constructed where Zr and Hf were replaced by Ti (0.25) atom (muffin-tin radii of Ti 2.13 au in the case of  $\text{ZrGeO}_4$  and 2.12 au in the case of  $\text{HfGeO}_4$  compound). With this supercell structure, we have calculated the electronic and optical properties to find the effect of doping on these properties with the TB-mBJ functional.

## RESULTS AND DISCUSSION

**Crystal Structure at Ambient Pressure.** The compounds  $\text{ZrGeO}_4$ ,  $\text{HfGeO}_4$  crystallize in tetragonal crystal structure with spacegroup  $I4_1/a$  (88) with 4(b) Wyckoff positions for M (Zr, Hf) atom and 4(a) and 16(f) for Ge, O atoms, respectively. The structure consists of an isolated  $\text{GeO}_4$  tetrahedron linked by 8-fold coordinated metal cation polyhedra.<sup>31,32</sup> The scheelite crystal structure of  $\text{HfGeO}_4$  is shown in Figure 1. As a first step,

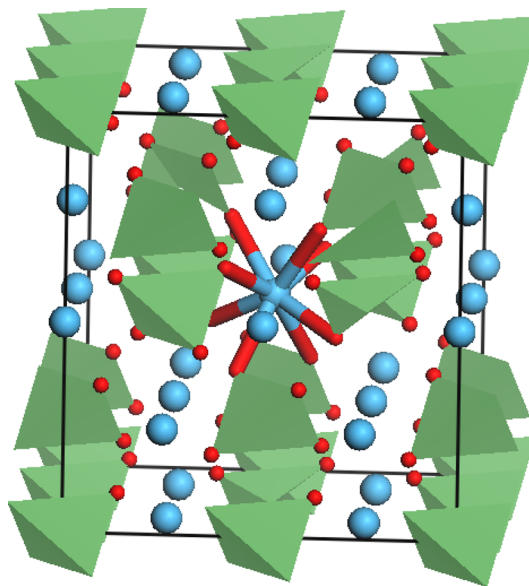


**Figure 1.** The scheelite crystal structure of  $\text{HfGeO}_4$ . Here, the blue ball indicates the Hf atom, the red ball indicates the O atom, and the Ge atom is within the tetrahedra.

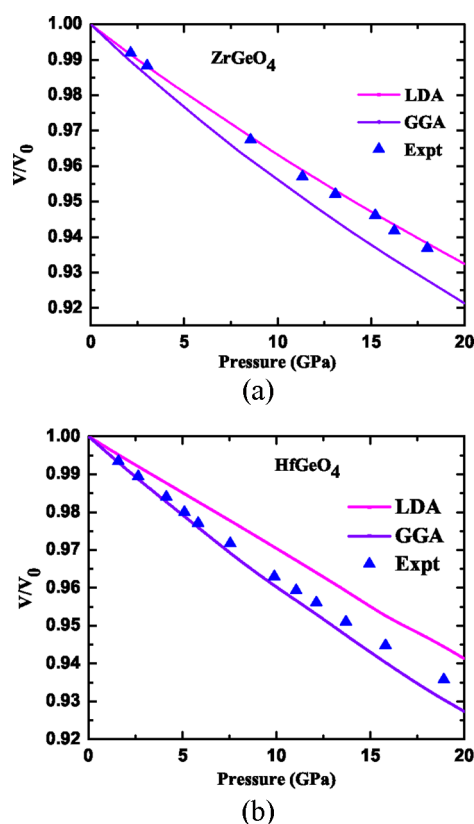
we have optimized the experimental crystal structure of both compounds  $\text{ZrGeO}_4$  and  $\text{HfGeO}_4$  by using LDA and GGA. The calculated equilibrium lattice parameters of both compounds using LDA and GGA exchange–correlation functionals are presented in Table 1 along with the experimental data. The difference between the computed and experimental volume is less within LDA as compared to GGA. The calculated volume at the LDA level is underestimated by 3.8%, 2.5%, whereas the GGA overestimated the volume by 3.2%, 8.3% for  $\text{ZrGeO}_4$  and  $\text{HfGeO}_4$  respectively. Therefore, for the ground-state structural properties of Zr- and Hf-based scheelite compounds, the agreement between the theoretical and experimental values is good with LDA over GGA. This is in good accord with the earlier theoretical reports on the scheelite structured compounds where LDA works well in the description of crystal structure.<sup>14</sup>

**Structural Properties under Pressure.** To study the effect of hydrostatic pressure on the crystal structure of  $\text{ZrGeO}_4$  and  $\text{HfGeO}_4$ , we have used the variable cell optimization technique as implemented in CASTEP code. We applied hydrostatic pressure up to 20 GPa. The external pressure was gradually increased by an increment of 2 GPa in each time. Under a given pressure, the internal coordinates and unit cell parameters of the germanate crystal were determined by minimizing the Hellmann–Feynman force on the atoms and the stress on the unit cell simultaneously. The computed pressure-normalized volume diagrams by using LDA and GGA along with experimental data are plotted in Figure 2a and b, respectively. Up to the studied pressure range of 20 GPa, the

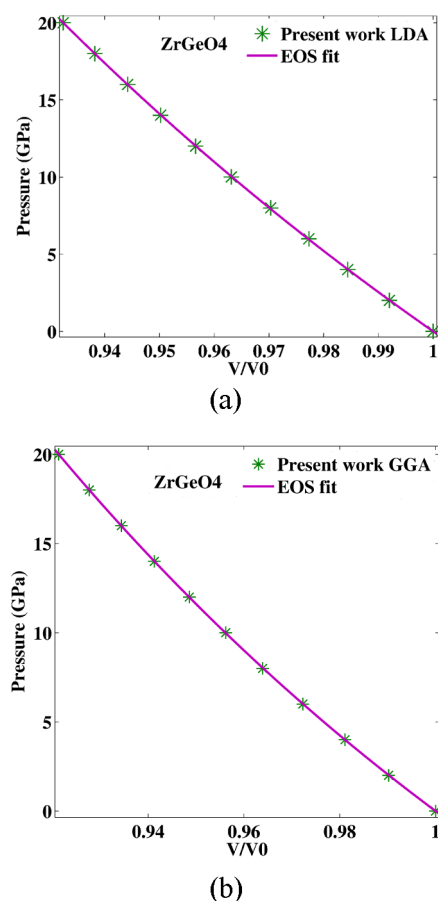
**Table 1.** Calculated Ground-State Properties of Tetragonal ZrGeO<sub>4</sub> and HfGeO<sub>4</sub> at Ambient Pressure

lattice parameter	LDA	GGA	expt
ZrGeO <sub>4</sub>			
<i>a</i> (Å)	4.804	4.910	4.866 <sup>a</sup>
<i>b</i> (Å)	4.804	4.910	4.866 <sup>a</sup>
<i>c</i> (Å)	10.406	10.694	10.550 <sup>a</sup>
<i>V</i> (Å <sup>3</sup> )	240.2	257.8	249.8
Zr	(0, 0, 0.5)	(0, 0, 0.5)	(0, 0, 0.5) <sup>a</sup>
Ge	(0, 0, 0)	(0, 0, 0)	(0, 0, 0) <sup>a</sup>
O	(0.2541, 0.1613, 0.0634)	(0.2568, 0.8143, 0.0575)	(0.2664, 0.1726, 0.0822) <sup>a</sup>
HfGeO <sub>4</sub>			
<i>a</i> (Å)	4.805	4.982	4.862 <sup>b</sup>
<i>b</i> (Å)	4.805	4.982	4.862 <sup>b</sup>
<i>c</i> (Å)	10.472	10.83	10.497 <sup>b</sup>
<i>V</i> (Å <sup>3</sup> )	241.8	268.9	248.1 <sup>b</sup>
Hf	(0, 0, 0.5)	(0, 0, 0.5)	(0, 0, 0.5) <sup>b</sup>
Ge	(0, 0, 0)	(0, 0, 0)	(0, 0, 0) <sup>b</sup>
O	(0.2607, 0.1656, 0.0830)	(0.2514, 0.1645, 0.0681)	(0.2678, 0.1739, 0.0831) <sup>b</sup>

<sup>a</sup>Reference 31. <sup>b</sup>Reference 32.

**Figure 2.** Pressure versus  $V/V_0$  of (a) ZrGeO<sub>4</sub> and (b) HfGeO<sub>4</sub>.

volume reduction  $V/V_0$  is approximately 7% in LDA and 8% in GGA for both of the compounds. It should be noted that for both of the compounds, LDA works well at ambient conditions, and as pressure increases, GGA values are found to be in close agreement with experiments for HfGeO<sub>4</sub>. The computed pressure volume–data have been fitted to the Murnaghan equation of state (EOS). The corresponding figures are shown in Figure 3a,b within LDA and GGA, respectively, for ZrGeO<sub>4</sub>,

**Figure 3.** Pressure versus  $V/V_0$  of ZrGeO<sub>4</sub>: (a) LDA and (b) GGA fitted with Murnaghan equation of state.

and in Figure 4a and b, we have shown them for HfGeO<sub>4</sub>. The bulk modulus  $B$  and its pressure derivative  $B_0'$  are found to be  $B_0 = 247.7$  GPa,  $B_0' = 3.985$  in LDA and  $B_0 = 200.1$  GPa,  $B_0' = 4.692$  in GGA for ZrGeO<sub>4</sub>, whereas  $B_0 = 265.7$  GPa,  $B_0' = 4.473$  in LDA and  $B_0 = 226.5$  GPa,  $B_0' = 4.044$  in GGA for HfGeO<sub>4</sub>, respectively. The high bulk modulus of the compound results in low compressibility. The bulk modulus values of these compounds are found to be greater than those of other scheelite-type compounds CaWO<sub>4</sub> (74 GPa),<sup>11</sup> SrWO<sub>4</sub> (63 GPa),<sup>11</sup> PbWO<sub>4</sub> (66 GPa),<sup>11</sup> and ThGeO<sub>4</sub> (183 GPa).<sup>14</sup> Therefore, both of these compounds are hard and less compressible than the above-mentioned scheelite compounds.

The variation of lattice parameters  $a$  and  $c$  with pressure are given in Figure 5a for ZrGeO<sub>4</sub> and in Figure 5b for HfGeO<sub>4</sub>, respectively, along with the experimental data. Clearly, the compression of Zr and Hf germanates is anisotropic as the lattice parameters have different compression behavior with pressure. For both of the compounds, the  $c$ -axis is 1.4% more compressible than the  $a$ -axis in LDA, whereas it is 1.6% in GGA. The compressibility of the lattice axis through LDA calculations is in good agreement with the experimental result, that is, 1.3% more compression of  $c$ -axis over  $a$ -axis. This anisotropy in the axial compressibility of scheelite (Zr and Hf) GeO<sub>4</sub> compounds is also observed in the other scheelite compounds such as ThGeO<sub>4</sub> and also for zircon, ZrSiO<sub>4</sub>. This may also be due to the fact that in both of the compounds Ge–O bonds are aligned along the  $a$ -axis. The Mulliken bond populations of Ge–O and M(Zr, Hf)–O are found to be 0.58,

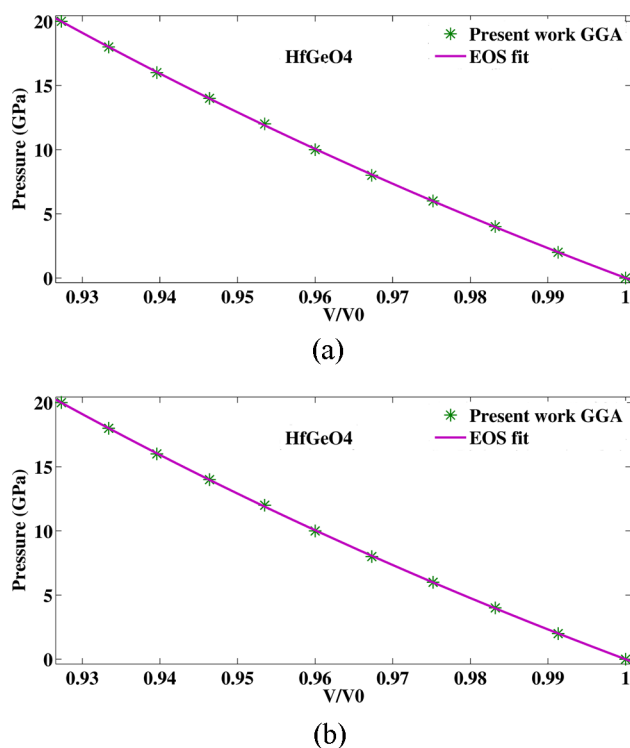


**Figure 4.** Pressure versus  $V/V_0$  of  $\text{HfGeO}_4$ : (a) LDA and (b) GGA fitted with Murnaghan's equation of state.

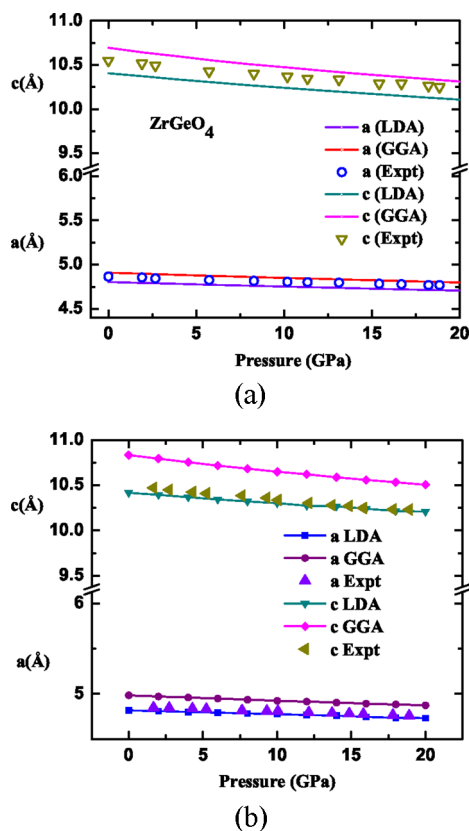


**Figure 5.** Variation of lattice parameters of (a)  $\text{ZrGeO}_4$  and (b)  $\text{HfGeO}_4$  with pressure.

0.34 for  $\text{ZrGeO}_4$  and 0.56, 0.40 for  $\text{HfGeO}_4$ , respectively. This clearly shows that both of the materials are covalent in nature.

**Bulk Modulus and Elastic Constants.** The elastic constants have been calculated to assess the mechanical stability of the studied compounds. Because the compounds have tetragonal crystal symmetry, there are six independent elastic constants,  $C_{11}$ ,  $C_{12}$ ,  $C_{13}$ ,  $C_{33}$ ,  $C_{44}$ , and  $C_{66}$ . The calculated elastic constants are presented in Table 2. To the best of our knowledge, there are no experimental data available to compare with the present values. The mechanical stability of the tetragonal crystal requires the whole set of elastic constants satisfying the Born–Huang criterion<sup>33</sup> given by  $C_{11} > 0$ ,  $C_{33} > 0$ ,  $C_{44} > 0$ ,  $C_{66} > 0$ ,  $(C_{11} - C_{12}) > 0$ ,  $(C_{11} + C_{33} - 2C_{13}) > 0$ , and  $[2(C_{11} + C_{12}) + C_{33} + 4C_{13}] > 0$ . Clearly, the calculated elastic constants satisfy all of the stability criteria indicating the scheelite-type structured Zr and Hf germanates to be mechanically stable systems. The bulk modulus of the compounds is calculated by using the elastic constants data, and the value is given in Table 2. The calculated bulk modulus of both of the compounds is in fair agreement with the experimental values. The calculated bulk moduli from the elastic constants agree well with those directly obtained from the fitting of the pressure–volume data to the Murnaghan EOS. It should be noted that the computed bulk modulus value of  $\text{ZrGeO}_4$  ( $B = 245.2$  GPa) is higher than that of zircon  $\text{ZrSiO}_4$  ( $B = 225.2$  GPa) but lower when compared to  $\text{HfGeO}_4$  ( $B = 266.6$  GPa).

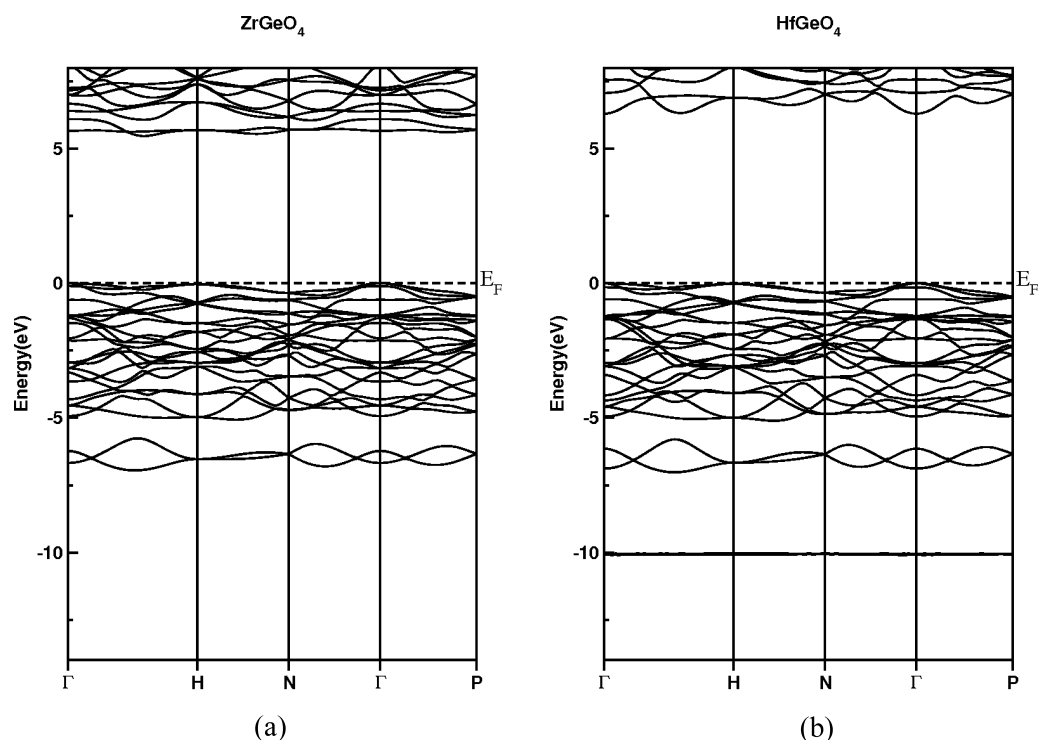
**Electronic Properties.** It is well-known that the scheelite structured  $\text{ABO}_4$  compounds are wide band gap semiconductors.<sup>8</sup> To the best of our knowledge, there are no studies available on electronic structure and optical properties of the scheelite structured germanates  $\text{ZrGeO}_4$  and  $\text{HfGeO}_4$ . The electronic band structures of the  $\text{ZrGeO}_4$  and  $\text{HfGeO}_4$  have been calculated using three different exchange–correlation functionals, GGA-PBE, EV-GGA, and TB-mBJ as implemented in WIEN2k code. Among these functionals, the TB-mBJ functional results in improving the energy gaps when compared to experiment. Koller et al. calculated the electronic band gaps of semiconducting transition metal oxides using the TB-mBJ functional, which are in very good agreement with experiments.<sup>30</sup> Recently, Dixit et al. calculated electronic band structures of binary and ternary oxides using the TB-mBJ potential along with GW calculations. Their study concludes that the calculated band gaps compare well with those obtained from GW calculations and also with experiment.<sup>34</sup> Camargo-Martinez et al. calculated the electronic band gaps of different types of semiconductors and insulators using the TB-mBJ functional, which are consistent with experimental results.<sup>35</sup> Therefore, in this study, we have used the TB-mBJ functional to determine the exact band gap values of  $\text{ZrGeO}_4$  and  $\text{HfGeO}_4$  compounds besides the usual PBE and EV functionals. The calculated electronic band structures of the germanates along high symmetry directions are shown in Figure 6a and b, respectively. The computed band structures clearly show that  $\text{ZrGeO}_4$  has the band gap of 5.39 eV, whereas  $\text{HfGeO}_4$  has the band gap of 6.25 eV, respectively. One should notice that the valence band maxima (VBM) and conduction band minima (CBM) are located at  $\Gamma$  point for  $\text{HfGeO}_4$  leaving the compound as a direct band gap insulator, whereas  $\text{ZrGeO}_4$  is an indirect gap material as VBM and CBM occur along  $\Gamma$  and  $H$ , respectively. The band gaps calculated using the three exchange correlational functionals GGA-PBE, EV-GGA, and TB-mBJ are presented in Table 3.

The calculated densities of states (DOS) for the investigated compounds are shown in Figure 7a and b, respectively, which

**Table 2.** Single-Crystal Elastic Constants ( $C_{ij}$  in GPa) and Bulk Modulus  $B$  (GPa) of  $ZrGeO_4$  and  $HfGeO_4$  Calculated at the Theoretical Equilibrium Volume within LDA

compound	$C_{11}$	$C_{12}$	$C_{13}$	$C_{33}$	$C_{44}$	$C_{66}$	$B$
$ZrGeO_4$	444.9	190.9	151.5	365.8	82.9	113.3	245.2 [229.4] <sup>a</sup> (238) <sup>b</sup>
$HfGeO_4$	447.5	209.6	177.5	397.5	95.9	128.1	266.6 [235.7] <sup>a</sup> (242) <sup>b</sup>

<sup>a</sup>The bulk modulus value calculated within GGA. <sup>b</sup>Reference 13.

**Figure 6.** Calculated band structure of  $MGeO_4$  ( $M = Zr, Hf$ ) along the high symmetry directions using the TB-mBJ functional at the experimental lattice constants.**Table 3.** Calculated Band Gap, in eV, of  $MGeO_4$  ( $M = Zr, Hf$ ) Compounds Using GGA, EV, and TB-mBJ Functionals at the Experimental Lattice Constants

method	$ZrGeO_4$	$HfGeO_4$
GGA	4.03	4.29
EV	4.28	4.66
TB-mBJ	5.39	6.25

are helpful in identifying the character of band states at different energy levels. The DOS plots show two upper and middle valence bands in the case of  $ZrGeO_4$  compound and three bands, upper valence band, middle valence band, and lower valence band, in the case of  $HfGeO_4$ . For both of the compounds, the upper valence band is formed due to hybridization of O-p states, Ge-p, and M (Hf, and Zr)-d states around the energy range  $-5$  to  $0$  eV, the middle valence band is mostly from Ge-s and O-p states situated around the energy range of  $-7.0$  to  $-5.7$  eV, and an extra lower valence band is present in the case of  $HfGeO_4$  when compared to  $ZrGeO_4$  due to the presence of extra f-electrons in Hf around the energy range from  $-10$  to  $-9.4$  eV. We found strong hybridization of Ge-p, O-p states, which reveal the covalent bond between the Ge and O atoms. In both cases, the conduction band is formed due to the d-states of Zr and Hf metal atoms.

To know the effect of Ti doping on the electronic structure properties, we have calculated the partial density of states with

Ti-doped  $ZrGeO_4$  and  $HfGeO_4$ , and the corresponding figures are shown in Figure 7c and d, respectively. We observed the additional Ti-d states are present in the energy gap of the host compound around the energy range  $3.2$ – $4.9$  eV for  $ZrGeO_4$  compound and  $3.3$ – $4.5$  eV for  $HfGeO_4$  compound, thereby reducing the original band gap of these compounds to  $3.2$  and  $3.3$  eV for  $ZrGeO_4$ ,  $HfGeO_4$  compounds, respectively.

**Optical Properties.** Optical properties of  $ZrGeO_4$  and  $HfGeO_4$  have been studied by using the TB-mBJ potential. To calculate the optical properties, we have used a denser  $k$ -point grid of  $18 \times 18 \times 18$  to arrive at the accurate optical properties. The complex dielectric function ( $\epsilon(\omega) = \epsilon_1(\omega) + i\epsilon_2(\omega)$ ), which gives the response of the material to external photon perturbation, consists of real and imaginary parts. The real part of the dielectric function  $\epsilon_1$  can be calculated from the imaginary part by using the Kramers–Kronig relations, and the knowledge of both the real and the imaginary parts of the dielectric function allows the calculation of important optical properties such as refractive index, reflectivity, and absorption coefficients. The calculated absorptive part  $\epsilon_2(\omega)$  and the dispersive part  $\epsilon_1(\omega)$  of the complex dielectric function as a function of photon energy are shown in Figure 8a and b, respectively. In the imaginary part of the dielectric function, the threshold energy increases from Zr to Hf because of the increase in the band gap values from Zr to Hf. The maximum value of the imaginary part of dielectric function is found to be

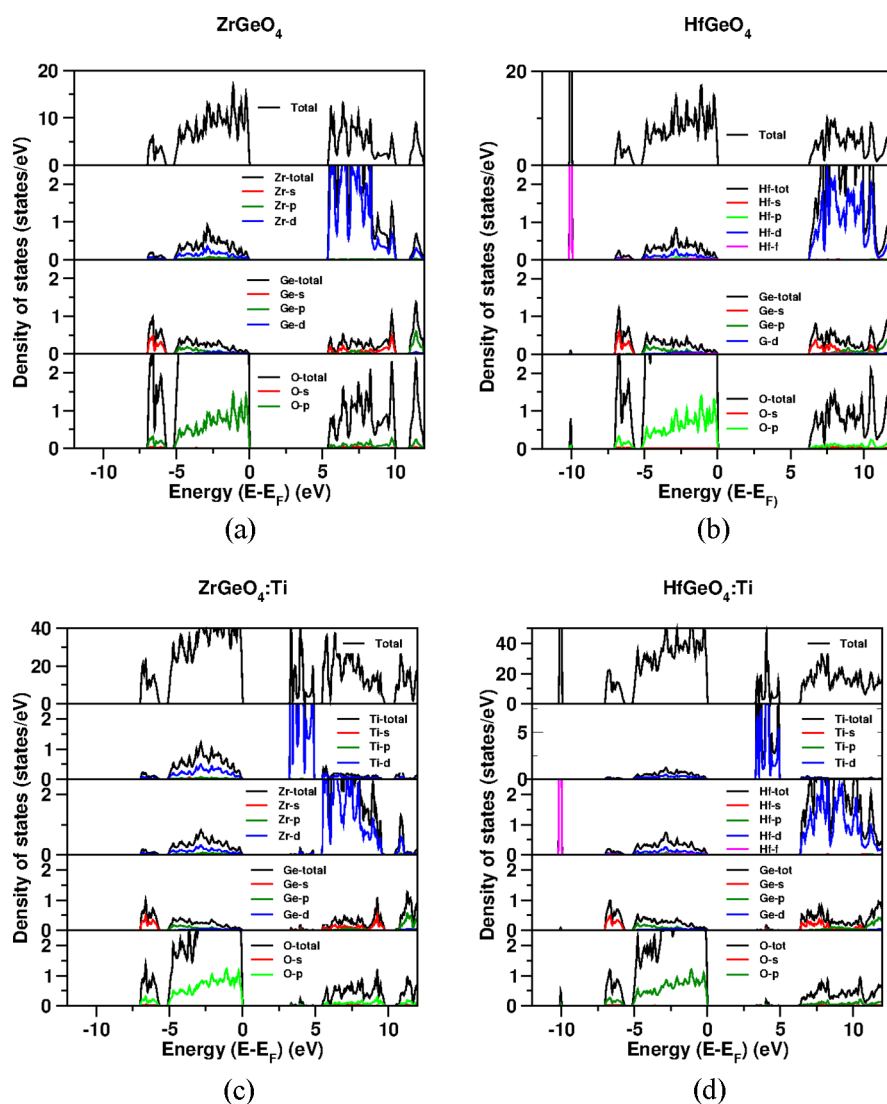


**Figure 7.** Total and partial density of states of (a)  $\text{ZrGeO}_4$ , (b)  $\text{HfGeO}_4$ , and Ti-doped (c)  $\text{ZrGeO}_4$  and (d)  $\text{HfGeO}_4$  compounds calculated using the TB-mBJ functional.

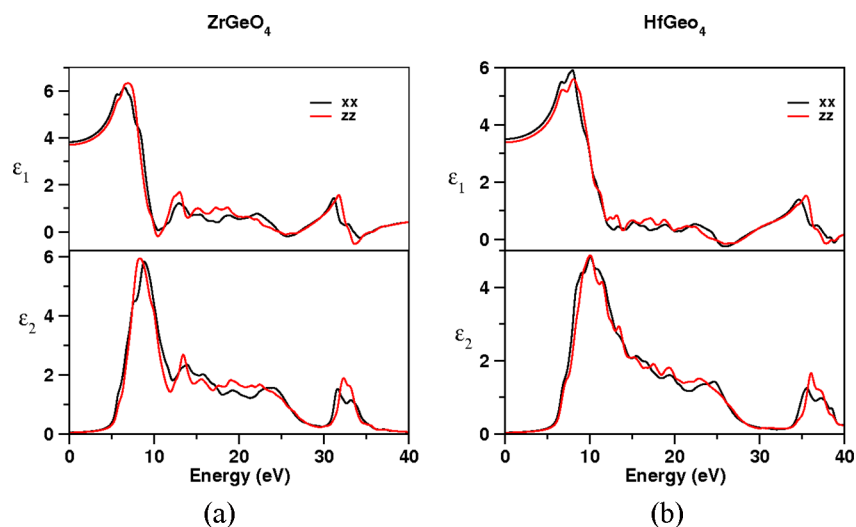


**Figure 8.** Calculated dielectric function of (a)  $\text{ZrGeO}_4$ , (b)  $\text{HfGeO}_4$  using TB-mBJ functional.

5.93 at energy of 8.34 eV in the case  $\text{ZrGeO}_4$ , while in the case of  $\text{HfGeO}_4$  the maximum value of 4.84 is reached at energy of

10 eV. It is known that the absorptive part of the dielectric function  $\epsilon_2(\omega)$  can be related to the band structure by means of

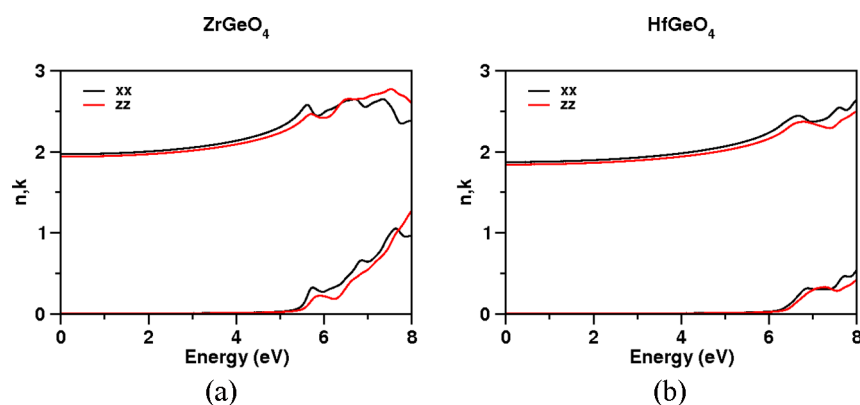


Figure 9. Calculated refractive index of (a)  $\text{ZrGeO}_4$ , (b)  $\text{HfGeO}_4$  using the TB-mBJ functional.

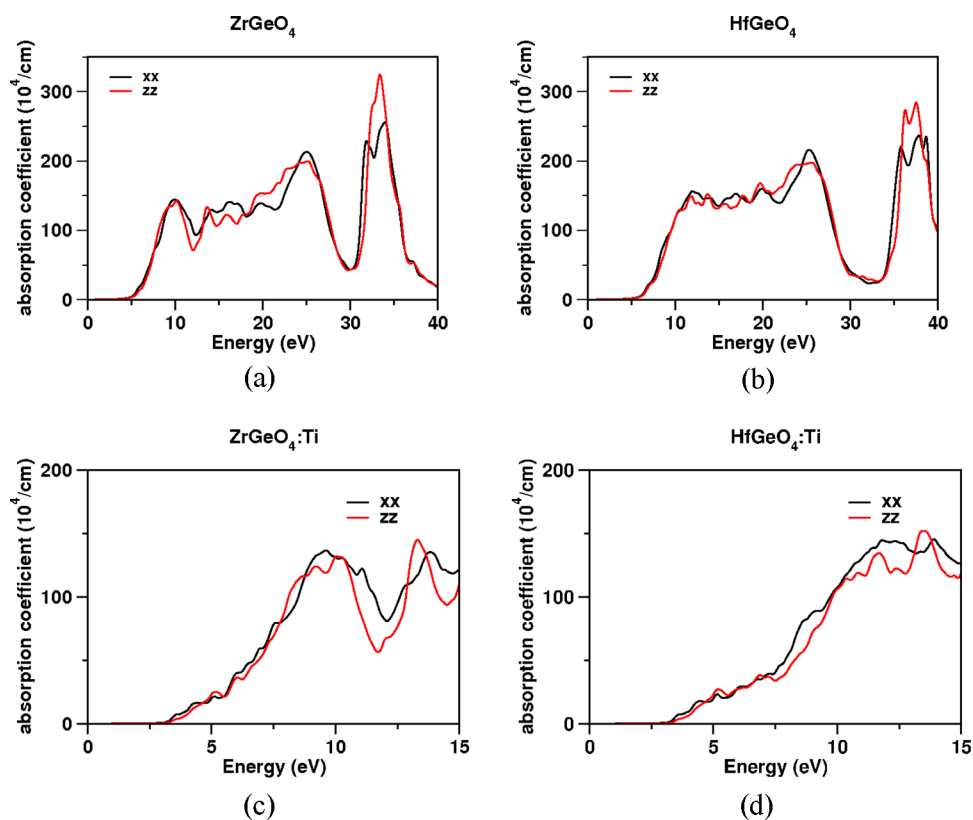


Figure 10. Absorption spectra of (a)  $\text{ZrGeO}_4$ , (b)  $\text{HfGeO}_4$ , (c)  $\text{ZrGeO}_4:\text{Ti}$ , and (d)  $\text{HfGeO}_4:\text{Ti}$  compounds using the TB-mBJ functional.

interband transitions. The calculated  $\epsilon_2(\omega)$  spectra of both of the germanates have different peaks at different photon energies, which are entirely due to the optical transitions from the occupied states (valence band) to unoccupied states (conduction band). The sharp peak observed at 8.34 eV in  $\text{ZrGeO}_4$  and at 10 eV in  $\text{HfGeO}_4$  may be due to the transition from the “p” states of O to the “d” states of Zr. The calculated dispersive part of dielectric function  $\epsilon_1(\omega)$  clearly shows that both of the germanates are optically anisotropic materials and the static values of  $\epsilon_1(\omega)$  are given by 3.82 and 3.70 for the compound  $\text{ZrGeO}_4$  along the  $x$ ,  $z$  directions and 3.49, 3.38 for the compound  $\text{HfGeO}_4$ , respectively. The calculated  $\epsilon_1(\omega)$  is found to increase with photon energy and reaches a maximum value and then decreases with increase in the photon energy. We also calculated the refractive index “ $n$ ” and extinction coefficient “ $\kappa$ ” of the germanates as a function of incident photon energy, which are shown in Figure 9a and b,

respectively. The refractive index follows the opposite trend to that of the band gap. The static refractive index values of the compounds are 1.94, 1.855 for the  $\text{ZrGeO}_4$ ,  $\text{HfGeO}_4$  compounds, respectively, which is opposite to that of the band gap; that is, band gap values increase from Zr to Hf. The calculated frequency-dependent absorption coefficient is shown in Figure 10a and b, which is directly proportional to the imaginary part of dielectric function. From Figure 10a and b, it is clearly seen that the absorption edge moves to higher energies as we move from Zr to Hf because of the increase in the band gap values from  $\text{ZrGeO}_4$  to  $\text{HfGeO}_4$ . For both of the compounds, we observed the absorption spectra mostly in the region 6–40 eV, that is, in the ultraviolet region.

It is reported that  $\text{MGeO}_4:\text{Ti}$  ( $\text{M} = \text{Zr}$  and  $\text{Hf}$ ) are good phosphors.<sup>2,4</sup> To study the effect of Ti addition on these compounds, we have calculated the electronic and optical properties of  $\text{ZrGeO}_4$  and  $\text{HfGeO}_4$  with Ti doping. We

observed the doped Ti states near the conduction band as shown in Figure 7c and d. Similar results are also obtained in the first principles study of  $\text{HfO}_2\text{:Ti}^{36}$  where the impurity states formed are near the bottom of the conduction band leading to the reduction in the band gap; moreover, it is also found that  $\text{HfO}_2\text{:Ti}$  is a good phosphor. In our present study, we also observed the band gap to reduce with the addition of Ti. We have also calculated the absorption spectra of Ti-doped  $\text{ZrGeO}_4$  and  $\text{HfGeO}_4$  compound as shown in Figure 10c and d and found the spectra shift to a lower energy region as compared to the host compound. As a result, we may expect the emission spectra to be in the visible region, which might be a reason for these compounds to be a good phosphor with the addition of Ti.

**Vibrational Properties.** Vibrational properties are obtained by the use of linear response method within the density functional perturbation theory (DFPT).<sup>37,38</sup> In this method, the force constants matrix can be obtained by differentiating the Hellmann–Feynman forces on atoms with respect to the ionic coordinates. This means that the force constant matrix depends on the ground-state electron charge density and on its linear response to a displacement of the atoms. By variational principle, the second-order change in energy depends on the first-order change in the electron density, and this can be obtained by minimizing the second-order perturbation in energy, which gives the first-order changes in the density, wave functions, and potential. In the present study, elements of the dynamical matrix are calculated on the  $4 \times 4 \times 4$  grid of  $k$ -points using the linear response approach. The primitive cell of the germanates contains 2 formula units, and hence there are 36 vibration modes. Out of these 36 modes, three are acoustic modes and the remaining 33 are optical modes. The following shows the details of group theory symmetry decomposition of the modes: acoustic modes,  $A_u + 2E_u$ , and optical modes,  $8E_u + 4A_u + 3B_u + 10E_g + 5B_g + 3A_g$ . In these modes,  $E_u$  and  $A_u$  are infrared active, whereas  $E_g$ ,  $B_g$ , and  $A_g$  modes are Raman active and  $B_u$  modes are silent. The calculated vibrational frequencies are presented in Table 4 along with the experimental Raman frequencies values of  $\text{ZrGeO}_4$ . In the case of the present germanates, there are in total 13 Raman active phonon modes  $3A_g + 5B_g + 5E_g$ . Out of these 13 modes, seven are internal modes of  $\text{GeO}_4$  tetrahedra. The modes with frequencies  $811.3 \text{ cm}^{-1}$  ( $A_g$ ),  $790.4 \text{ cm}^{-1}$  ( $E_g$ ), and the mode at  $732.4 \text{ cm}^{-1}$  ( $B_g$ ) in  $\text{ZrGeO}_4$  and the modes with frequencies  $830.1 \text{ cm}^{-1}$  ( $A_g$ ),  $826.1 \text{ cm}^{-1}$  ( $E_g$ ), and the mode with frequency  $766.3 \text{ cm}^{-1}$  ( $B_g$ ) in  $\text{HfGeO}_4$  are due to the stretching of Ge–O bonds, respectively. The bending modes are situated at  $414.8 \text{ cm}^{-1}$  ( $A_g$ ),  $425.6 \text{ cm}^{-1}$  ( $B_g$ ),  $610.7 \text{ cm}^{-1}$  ( $B_g$ ), and  $538.7 \text{ cm}^{-1}$  ( $E_g$ ) in  $\text{ZrGeO}_4$  and  $383.2 \text{ cm}^{-1}$  ( $A_g$ ),  $401.1 \text{ cm}^{-1}$  ( $B_g$ ),  $564.4 \text{ cm}^{-1}$  ( $B_g$ ), and  $497.6 \text{ cm}^{-1}$  ( $E_g$ ) in  $\text{HfGeO}_4$ , respectively. The remaining six modes are rotational ( $A_g$  and  $E_g$ ) and translational modes ( $2B_g$  and  $2E_g$ ).

## CONCLUSION

We have studied the high-pressure structural stability, elastic constants, and vibrational properties of scheelite-type  $\text{MGeO}_4$  ( $M = \text{Zr, Hf}$ ) compounds, which are good X-ray phosphors by using planewave pseudopotential method and electronic and optical properties using full potential linearized augmented plane wave method. We found that there is no structural phase transition until the studied pressure range of 20 GPa, which is in good agreement with the experiment. We also noticed that both of the compounds are highly incompressible, and it is

**Table 4. Vibrational Frequencies of  $\text{ZrGeO}_4$  and  $\text{HfGeO}_4$  Calculated at Theoretical Equilibrium Volume within LDA. Here RA refers to Raman Active and IA refers to Infrared Active**

mode	$\text{ZrGeO}_4$ (ref 4)	mode	$\text{HfGeO}_4$
$B_g$	167.3 (171) (RA)	$E_g$	153.0 (RA)
$E_g$	180.5 (182) (RA)	$B_g$	157.1 (RA)
$A_u$	194.1 (IA)	$A_u$	174.9 (IA)
$E_u$	196.9 (IA)	$E_u$	204.6 (IA)
$E_g$	252.7 (255) (RA)	$E_g$	246.3 (RA)
$A_g$	288.6 (294) (RA)	$E_u$	269.6 (IA)
$A_u$	292.4 (IA)	$B_g$	269.9 (RA)
$E_u$	299.7 (IA)	$A_u$	294.3 (IA)
$B_g$	317.8 (306) (RA)	$A_g$	306.2 (RA)
$B_u$	340.2	$B_u$	366.1
$A_g$	383.2 (378) (RA)	$E_g$	398.3 (RA)
$E_g$	384.4 (368) (RA)	$A_g$	414.8 (RA)
$B_g$	404.1 (406) (RA)	$B_g$	425.6 (RA)
$E_u$	439.3 (IA)	$E_u$	479.4 (IA)
$E_g$	497.6 (495) (RA)	$E_g$	538.7 (RA)
$A_u$	527.9 (IA)	$A_u$	553.3 (IA)
$B_g$	564.4 (565) (RA)	$B_g$	610.7 (RA)
$B_u$	630.6	$B_u$	676.0
$E_u$	712.4 (IA)	$E_u$	724.4 (IA)
$A_u$	716.1 (IA)	$A_u$	741.2 (IA)
$B_g$	732.4 (729) (RA)	$B_g$	766.3 (RA)
$B_u$	781.7	$B_u$	793.7
$E_g$	790.4 (782) (RA)	$E_g$	826.1 (RA)
$A_g$	811.3 (802) (RA)	$A_g$	830.1 (RA)

found to be more compressible along the  $c$ -axis than along the  $a$ -axis, which might be due to the presence of a strong covalent Ge–O bond along  $a$ -axis. This fact is also confirmed from the calculated elastic constants, which follow the order  $C_{11} > C_{33}$ . In addition, we have also calculated the vibrational properties and discussed the Raman and IR frequencies of the germanates, which are in reasonable agreement with the experiment. The investigated germanate compounds are found to be insulators, and the band gap is more for  $\text{HfGeO}_4$  than for  $\text{ZrGeO}_4$ . The optical properties were calculated and analyzed through the computed band structures. We also studied the doping effect of Ti on electronic structure, and we found this doped state to be near the conduction band edge. As a result, the band gap of these compounds decreases, and we also observed the absorption spectra to shift to lower energy regions, leading to the expectation that the emission spectra may be in the visible range, which might be a reason for these compounds to be good X-ray phosphors when doped with Ti.

## AUTHOR INFORMATION

### Corresponding Author

\*E-mail: kanchana@iith.ac.in.

### Notes

The authors declare no competing financial interest.

## ACKNOWLEDGMENTS

V.K. would like to acknowledge IIT Hyderabad for the HPC facility and NSFC awarded Research Fellowship for International Young Scientists under Grant No. 11250110051. G.S. would like to acknowledge IIT Hyderabad for computational facility and MHRD for the fellowship. K.R.B. and G.V. thank the Center for Modelling Simulation and Design, University of

Hyderabad (CMSD-UoH), for providing a computational facility.

## REFERENCES

- (1) Nikl, M. Scintillation Detectors for X-rays. *Meas. Sci. Technol.* **2006**, *17*, R37–R54.
- (2) Lambert, P. M. Synthesis of the  $\text{HfGeO}_4\text{:Ti}^{4+}$  X-ray Phosphor. *Mater. Res. Bull.* **2000**, *35*, 383–391.
- (3) Issler, S. L.; Torardi, C. C. Solid State Chemistry and Luminescence of X-ray Phosphors. *J. Alloys Compd.* **1995**, *229*, 54–65.
- (4) Tuschel, D. D.; Lambert, P. M. Site Occupancy of  $\text{Ti}^{4+}$ -doped  $\text{ZrGeO}_4$  and  $\text{HfGeO}_4$  Probed by Raman Spectroscopy. *Chem. Mater.* **1997**, *9*, 2852–2860.
- (5) Annenkov, A. A.; Korzhik, M. V.; Lecoq, P. Lead Tungstate Scintillation Material. *Nucl. Instrum. Methods Phys. Res. A* **2002**, *490*, 30–50.
- (6) Paski, E. F.; Blades, M. W. Analysis of Inorganic Powders by Time-wavelength Resolved Luminescence Spectroscopy. *Anal. Chem.* **1988**, *60*, 1224–1230.
- (7) Faure, N.; Borel, C.; Couchaud, M.; Basset, G.; Templier, R.; Wyon, C. Optical Properties and Laser Performance of Neodymium Doped Scheelites  $\text{CaWO}_4$  and  $\text{NaGd}(\text{WO}_4)_2$ . *Appl. Phys. B* **1996**, *63*, 593–598.
- (8) Errandonea, D.; Manjón, F. J. Pressure Effects on the Structural and Electronic Properties of  $\text{ABX}_4$  Scintillating Crystals. *Prog. Mater. Sci.* **2008**, *53*, 711–773.
- (9) Grzechnik, A.; Crichton, W. A.; Marshall, W. G.; Friese, K. High-pressure X-ray and Neutron Powder Diffraction Study of  $\text{PbWO}_4$  and  $\text{BaWO}_4$  Scheelites. *J. Phys.: Condens. Matter* **2006**, *18*, 3017–3029.
- (10) Panchal, V.; Garg, N.; Chauhan, A. K.; Sangeeta; Sharma, S. M. High Pressure Phase Transitions in  $\text{BaWO}_4$ . *Solid State Commun.* **2004**, *130*, 203–208.
- (11) Errandonea, D.; Pellicer-Porres, J.; Manjón, F. J.; Segura, A.; et al. High-pressure Structural Study of the Scheelite Tungstates  $\text{CaWO}_4$  and  $\text{SrWO}_4$ . *Phys. Rev. B* **2005**, *72*, 174106–14.
- (12) Errandonea, D.; Somayazulu, M.; Häusermann, D. Phase Transitions and Amorphization of  $\text{CaWO}_4$  at High Pressure. *Phys. Status Solidi b* **2003**, *235*, 162–169.
- (13) Panchal, V.; Garg, N.; Achary, S. N.; Tyagi, A. K.; Sharma, S. M. Equation of State of Scheelite-structured  $\text{ZrGeO}_4$  and  $\text{HfGeO}_4$ . *J. Phys.: Condens. Matter* **2006**, *18*, 8241–8250.
- (14) Errandonea, D.; Kumar, R. S.; Gracia, L.; Beltrán, A.; Achary, S. N.; Tyagi, A. K. Experimental and Theoretical Investigation of  $\text{ThGeO}_4$  at High Pressure. *Phys. Rev. B* **2009**, *80*, 094101–7.
- (15) Segall, M. D.; Lindan, P. J. D.; Probert, M. J.; Pickard, C. J.; Hasnip, P. J.; Clark, S. J.; Payne, M. C. First-principles Simulation: Ideas, Illustrations and the CASTEP Code. *J. Phys.: Condens. Matter* **2002**, *14*, 2717–2744.
- (16) Clark, S. J.; Segall, M. D.; Pickard, C. J.; Hasnip, P. J.; Probert, M. I. J.; Refson, K.; Payne, M. C. First Principles Methods Using CASTEP. *Z. Kristallogr.* **2005**, *220*, 567–570.
- (17) Payne, M. C.; Teter, M. P.; Allan, D. C.; Arias, T. A.; Joannopoulos, J. D. Iterative Minimization Techniques for Ab Initio Total-energy Calculations: Molecular Dynamics and Conjugate Gradients. *Rev. Mod. Phys.* **1992**, *64*, 1045–1097.
- (18) Vanderbilt, D. Soft Self-consistent Pseudopotentials in a Generalized Eigenvalue Formalism. *Phys. Rev. B* **1990**, *41*, 7892–7895.
- (19) Kresse, G.; Furthmüller, J. Efficient Iterative Schemes for ab initio Total-energy Calculations Using a Plane-wave Basis Set. *Phys. Rev. B* **1996**, *54*, 11169–11186.
- (20) Fischer, T. H.; Almlöf, J. General Methods for Geometry and Wave Function Optimization. *J. Phys. Chem.* **1992**, *96*, 9768–9774.
- (21) Ceperley, D. M.; Alder, B. J. Ground State of the Electron Gas by a Stochastic Method. *Phys. Rev. Lett.* **1980**, *45*, 566–569.
- (22) Perdew, J. P.; Zunger, A. Self-Interaction Correction to Density-Functional Approximations for Many-electron Systems. *Phys. Rev. B* **1981**, *23*, 5048–5079.
- (23) Perdew, J. P.; Burke, K.; Ernzerhof, M. Generalized Gradient Approximation Made Simple. *Phys. Rev. Lett.* **1996**, *77*, 3865–3868.
- (24) Monkhorst, H. J.; Pack, J. D. Special Points for Brillouin-zone Integrations. *Phys. Rev. B* **1976**, *13*, 5188–5192.
- (25) Mehl, M. J.; Osburn, J. E.; Papaconstantopoulos, D. A.; Klein, B. M. Structural Properties of Ordered High-melting-temperature Intermetallic Alloys from First-principles Total-energy Calculations. *Phys. Rev. B* **1990**, *41*, 10311–10323.
- (26) Blaha, P.; Schwarz, K.; Sorantin, P.; Tricky, S. B. Full-potential, Linearized Augmented Plane Wave Programs for Crystalline Systems. *Comput. Phys. Commun.* **1990**, *59*, 399–415.
- (27) Blaha, P.; Schwarz, K.; Madsen, G. K. H.; Kvasnicka, D.; Luitz, J. *WIEN2K, An Augmented Plane Wave Plus Local Orbitals Program for Calculating Crystal Properties*; Karlheinz Schwarz, Techn. Universität Wien: Austria, 2001.
- (28) Engel, E.; Vosko, S. H. Exact Exchange-only Potentials and the Virial Relation as Microscopic Criteria for Generalized Gradient Approximations. *Phys. Rev. B* **1993**, *47*, 13164–13174.
- (29) Singh, D. J. Electronic Structure Calculations With the Tran-Blaha Modified Becke-Johnson Density Functional. *Phys. Rev. B* **2010**, *82*, 205102–10.
- (30) Koller, D.; Tran, F.; Blaha, P. Merits and Limits of the Modified Becke-Johnson Exchange Potential. *Phys. Rev. B* **2011**, *83*, 195134–10.
- (31) Ennaciri, A.; Michel, D.; Perez y Jorba, M.; Pannetier, J. Neutron Diffraction Determination of the Structure of an Ordered Scheelite-type:  $\text{Zr}_3\text{GeO}_8$ . *Mater. Res. Bull.* **1984**, *19*, 793–799.
- (32) Ennaciri, A.; Kahn, A.; Michel, D. Crystal Structure of  $\text{HfGeO}_4$  and  $\text{ThGeO}_4$  Germanates. *J. Less-Common Met.* **1986**, *124*, 105–109.
- (33) Born, M.; Huang, K. *Dynamical Theory of Crystal Lattices*; Oxford University Press: Oxford, 1998.
- (34) Dixit, H.; Saniz, R.; Cottenier, S.; Lamoen, D.; Partoens, B. Electronic Structure of Transparent Oxides with the Tran-Blaha Modified Becke-Johnson Potential. *J. Phys.: Condens. Matter* **2012**, *24*, 205503–9.
- (35) Camargo-Martínez, J. A.; Baquero, R. Performance of the Modified Becke-Johnson Potential for Semiconductors. *Phys. Rev. B* **2012**, *86*, 195106–8.
- (36) Tan, T.; Liu, Z.; Li, Y. First-principles Calculations of Electronic and Optical Properties of Ti-doped Monoclinic  $\text{HfO}_2$ . *J. Alloys Compd.* **2012**, *510*, 78–82.
- (37) Gonze, X. First-principles Responses of Solids to Atomic Displacements and Homogeneous Electric Fields: Implementation of a Conjugate-gradient Algorithm. *Phys. Rev. B* **1997**, *55*, 10337–10354.
- (38) Refson, K.; Tulip, P. R.; Clark, S. J. Variational Density-functional Perturbation Theory for Dielectrics and Lattice Dynamics. *Phys. Rev. B* **2006**, *73*, 155114–12.